Metal-insulator transition in doped conjugated polymers: Effects of long-ranged Coulomb potentials

Kikuo Harigaya* and Akira Terai
Department of Physics, Faculty of Science, University of Tokyo, Hongo 7-3-1, Bunkyo-ku, Tokyo 113, Japan
(Received 29 January 1991)

The metal-insulator transition in doped conjugated polymers is investigated for charged impurities that are represented as long-ranged potentials. The impurity positions are randomly selected. The change in the number of electrons is determined by the number of impurities. Physical quantities are derived from a sufficiently large number of samples, each of which is described by a finite-size Su-Schrieffer-Heeger Hamiltonian with the impurity potentials. It is shown that the electronic gap can disappear above a certain concentration even as the dimerization patterns persist. The present results well explain the appearance of the metallic Pauli susceptibility, its magnitude, and the critical concentration, characteristic of the metal-insulator transition observed in experiments. The persistence of dimerization is also consistent with results of experiments in which highly doped samples are used. A comparison with a previous study using short-ranged site-type impurity models is given. It is found that the agreement is excellent, which indicates that the main results do not depend on whether the impurity potentials are short or long ranged.

I. INTRODUCTION

In a series of studies,[1-8] we have investigated how random impurities may affect the electronic structures of conjugated polymers. For the case in which the impurities give rise to isoelectronic disorders, we analyzed[1-6] the electronic states by the Takayama-Lin-Liu-Maki model,[9] using the coherent-potential approximation, and further by the Su-Schrieffer-Heeger (SSH) model,[10] making use of numerical diagonalization of finite systems.[7] Various changes found in the electronic structure have been reported. They depend on the type of the impurities and doping mechanisms. In a subsequent study,[8] the change in the number of electrons has been considered and the electronic structures have been investigated by a numerical method. Coulomb potentials due to the charged impurities have been assumed to be short ranged. They modulate the site energy at the impurity sites. The number of electrons is determined by the number of impurities. We have numerically diagonalized finite systems with randomly distributed impurities. Physical properties have been derived from calculated data of a sufficiently large number of samples. The most striking observation is that the energy gap at the Fermi level can vanish even as *the dimerization patterns persist.* This indicates an appearance of Pauli susceptibility and can partially explain the metal-insulator transition. The value of the critical concentration and impurity strength turned out to be reasonable for realistic, doped polyacetylene. The magnitude of the Pauli susceptibility is also comparable to the observed value.

Through the above studies, the impurity potentials have been assumed to be short ranged. A "site-type" impurity is effective on electrons only at one lattice site. A "bond-type" impurity modulates a hopping integral between a certain pair of CH units. Validity of the short-ranged impurities is evident, if screening by π electrons is *complete* and thus no long-ranged components remain. However, it might be possible that the screening is not complete in actual samples. The long-ranged components which are not completely screened might affect the electronic states.

The aim of the present paper is to examine effects of the *long-ranged impurity potentials.* Though there might be other possible forms of realistic Coulomb potentials, we consider the one used by Conwell and Jeyadev.[11] The dielectric constants are anisotropic, depending on whether the direction of each component is parallel or perpendicular to the chain. The component in the chain is larger because π electrons can move only in this direction. The dielectric constants are assumed to take values observed over the whole sample. They might be locally different near the impurities. Thus function forms of potentials around the impurities are different from those in regions far away from them. However, we assume the same form as in Ref. 11 because effects of long-ranged tails of the impurity potentials are expected to be qualitatively independent of the details of model potentials. We assume random configuration of impurities. In other words, we neglect the correlation effects among the impurities. The impurities are assumed to be of an acceptor type. The number of electrons is effectively decreased from half filling by the same number of impurities. For a given impurity distribution, the spatial variation of the dimerization amplitude and electronic states are numerically determined. Physical quantities are derived from the data for a sufficiently large number of samples. The numerical method is the same as that used in a previous study.[8]

The results of simulation are reported in the following order. First, properties of typical samples are discussed. For each sample, the spatial variation of the strength of impurity potentials, charge distribution, and lattice configuration are shown. Stationary configurations are

composed of various types of patterns: positive and negative solitons, positive- and negative-soliton lattices, and disruption of π conjugation. It is a consequence of the large spatial fluctuation of the impurity-potential strength. Next, the dimerization order parameter is averaged over a sufficiently large number of samples. An enhancement in dimerization over that in the impurity-free soliton-lattice system is reported. Finally, information about the electronic structures is derived. It is shown that the energy gap can vanish at an impurity concentration which is comparable to the observed magnitude.[12] The value of the density of states at the Fermi level is also of the same magnitude as the one observed.[12] Because of the absence of the electron-hole symmetry, the overall structures of density of states and plots of the inverse participation numbers are not symmetric with respect to the center of the energy. In the Appendix the present results are compared with our previous study of short-ranged site-type impurity problem.[8] It is shown that there are interesting and excellent one-to-one correspondences, making use of impurity strengths, critical concentrations, and correlation functions between the spatial variation of the potential strength and electron-density configuration. This implies that the disorder effects on the electronic properties do *not* sensitively depend on whether the impurity potentials are short or long ranged.

This paper is organized as follows. In Sec. II, the model and method of numerical simulation are presented. In Sec. III the simulation results are reported. Properties of typical samples are then discussed. Next, the information on physical quantities is derived and reported. We summarize the paper and discuss the results in Sec. IV. In the Appendix we compare the results with those of the short-ranged site-type impurity problem.

II. MODEL AND NUMERICAL METHOD

The SSH model is generalized to include terms which describe long-ranged potentials due to charged impurities. The Hamiltonian is given by

$$H=H_{\rm SSH}+H_{\rm imp} \ . \tag{2.1}$$

The first term is the original SSH-model Hamiltonian. Its form is

$$H_{\rm SSH}=-\sum_{n,s}[t_0-\alpha(u_{n+1}-u_n)](c^{\dagger}_{n+1,s}c_{n,s}+{\rm H.c.}) +\frac{K}{2}\sum_n (u_{n+1}-u_n)^2 \ , \tag{2.2}$$

where t_0 is the nearest-neighbor hopping integral of the undimerized chain, α the electron-phonon coupling strength due to the modulation of the hopping integral, u_n the displacement of the nth CH unit, $c_{n,s}$ an annihilation operator of an electron at the nth site with spin s, and K the force constant between adjacent units. The second term of Eq. (2.1) represents effects of the impurity potentials. They are given by

$$H_{\rm imp}=\sum_{n,s} V_n c^{\dagger}_{n,s}c_{n,s} \ , \tag{2.3}$$

$$V_n=\sum_{i,|i-n|\le N/2} V(n;i) \ , \tag{2.4}$$

and

$$V(n;i)=\frac{e^2}{\epsilon_{\perp}[(n-i)^2a^2+(\epsilon_{\parallel}/\epsilon_{\perp})d^2]^{1/2}} \ . \tag{2.5}$$

Equation (2.5) is an impurity potential centered at the ith site. This form was also used by Conwell and Jeyadev.[11] The quantity e is the magnitude of the unit charge, $\epsilon_{\perp}$ and $\epsilon_{\parallel}$ represent dielectric constants of perpendicular and parallel directions with respect to the chain, respectively, a is the lattice constant of the undimerized system, and d is the perpendicular distance between the chain and impurity chain. The form of (2.5) is the Fourier transform of the representation in the wave-number space:

$$V(q_{\parallel},q_{\perp})=\frac{4\pi e^2}{\epsilon_{\parallel}q_{\parallel}^2+\epsilon_{\perp}q_{\perp}^2} \ , \tag{2.6}$$

where $q_{\perp}$ and $q_{\parallel}$ are components of a wave vector perpendicular and parallel to the chain, respectively. Note that the lattice displacement u_n is neglected in (2.5), because it is much smaller than a: For instance, $|u_n|\sim 0.04$ Å, while $a\sim 1.2$ Å for the perfectly dimerized system. Even if u_n is included in (2.5), the results do not change apparently, because the impurity potential varies fairly slowly in the length scale of the order less than a. We define the quantity V_n by (2.4). It represents the total impurity strength at the nth site. The sum is taken over all the randomly distributed impurities. The restriction $|i-n|\le N/2$ is due to the periodic boundary condition. We consider an acceptor doping case by assuming the positive $V(n;i)$. When the number of lattice points N and the concentration c are given, the number of electrons $N_{\rm el}$ is determined by $N_{\rm el}=N-cN$. The periodic boundary conditions are imposed on electronic and lattice systems in order to remove end-point effects. When the κth wave function is expressed by $\phi_{\kappa}(n)$, it satisfied the boundary condition

$$\phi_{\kappa}(n+N)=\phi_{\kappa}(n) \ . \tag{2.7}$$

The boundary condition for the lattice is

$$u_{n+N}=u_n \ . \tag{2.8}$$

The eigenfunction $\phi_{\kappa}(n)$ is calculated from the Schrödinger equation

$$\varepsilon_{\kappa}\phi_{\kappa}(n)=-(t_0-\alpha y_{n-1})\phi_{\kappa}(n-1) -(t_0-\alpha y_n)\phi_{\kappa}(n+1)+V_n\phi_{\kappa}(n) \ , \tag{2.9}$$

where $y_n=u_{n+1}$ and ε_{κ} is the κth eigenvalue. The self-consistency condition for the lattice is

$$y=-\frac{2\alpha}{K}\sum_{\kappa,s}{}'\phi_{\kappa}(n+1)\phi_{\kappa}(n) +\frac{2\alpha}{KN}\sum_m\sum_{\kappa,s}{}'\phi_{\kappa}(m+1)\phi_{\kappa}(m) \ , \tag{2.10}$$

where the prime indicates a sum over occupied states and

the second term originates from the condition $\sum_n y_n = 0$ due to the periodic boundary condition (2.8).

A numerical solution is obtained in the following way.

(i) First, we choose cN impurity sites randomly out of N total lattice points and thus fix a sample.

(ii) Next, random numbers between $-y_0$ and y_0 ($y_0 = 0.1$ Å) are generated for the initial values of the bond variables $\{y_n^{(0)}\}$. Here we start the iteration.

(iii) At the kth step of the iteration, the electronic part of the Hamiltonian is diagonalized by solving Eq. (2.9) for the set of the bond variables $\{y_n^{(k)}\}$.

(iv) Using the electronic wave functions $\{\phi_\kappa(n)\}$ obtained above, we calculate the next set $\{y_n^{(k+1)}\}$ from the left-hand side of Eq. (2.10).

(v) The iteration is repeated until the sum $\sum_n [y_n^{(k+1)} - y_n^{(k)}]^2$ becomes sufficiently small.

III. SIMULATION RESULTS

Numerical investigations are performed for the parameters $\alpha = 4.1$ eV/Å, $K = 21$ eV/Å^2, and $t_0 = 2.5$ eV for the systems with $N = 100$. These give the dimensionless electron-phonon coupling constant $\lambda \equiv 2\alpha^2/\pi K t_0 = 0.20$. All the quantities with the dimension of the energy are given in the unit of t_0. Simulations are performed for two sets of dielectric constants. They are case A $\epsilon_\parallel = 7.08$ and $\epsilon_\perp = 1.77$ and case B $\epsilon_\parallel = 11.5$ and $\epsilon_\perp = 2.5$. These values have been used by Conwell and Jeyadev.[11] The dielectric constants within a distance of a few lattice constants from the impurity are not necessarily equal to the values observed over the whole sample. We, however, take those values in order to stimulate effects of the long-ranged impurity potential. Other parameters in (2.5) are $a = 1.22$ Å, $d = 2.4$ Å, and $e^2 = 14.3$ eV Å. The impurity concentration c is varied within the range $0.04 \le c \le 0.20$ for each case.

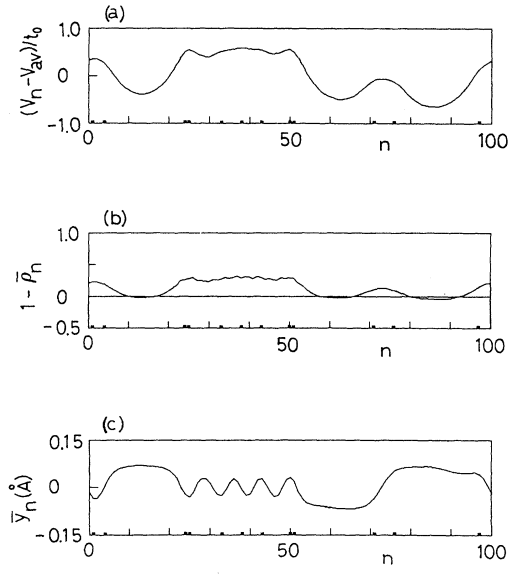

FIG. 1. (a) Spatial variation of the impurity potential $V_n - V_{av}$, where $V_{av} = (1/N)\sum_n V_n$, (b) the smoothed electron-density distribution $\bar{\rho}_n = (\rho_{n-1} + 2\rho_n + \rho_{n+1})/4$, and (c) the smoothed dimerization amplitude $\bar{y}_n = (-1)^n (y_n - y_{n+1})/2$ for a typical sample with long-ranged impurity-potentials. The dielectric constants are those of case A. The impurity concentration is $c = 0.12$. Positions of centers of the impurities are indicated by squares on the abscissa.

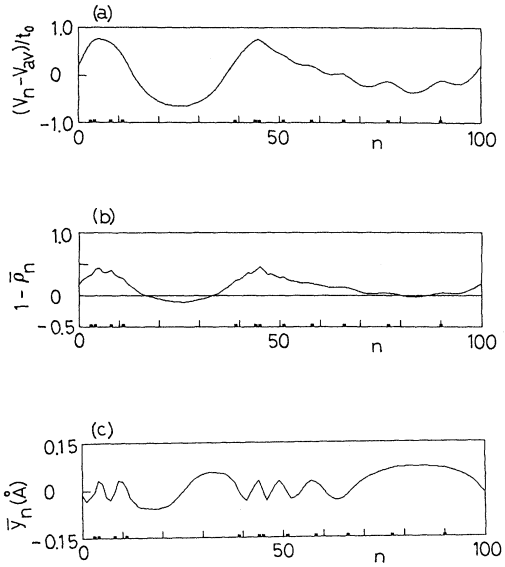

FIG. 2. Quantities $V_n - V_{av}$, $\bar{\rho}_n$, and $\bar{y}_n$ for another sample which is different from that in Fig. 1. Dielectric constants and the concentration are the same.

In Figs. 1–3 three typical solutions are presented for the case A and $c = 0.12$. In each figure part (a) shows spatial variation of the impurity potential $V_n - V_{av}$, where $V_{av} = (1/N)\sum_n V_n$. Positions of impurities are denoted by the squares on the abscissa. The strength V_n is larger in the regions where impurities are concentrated

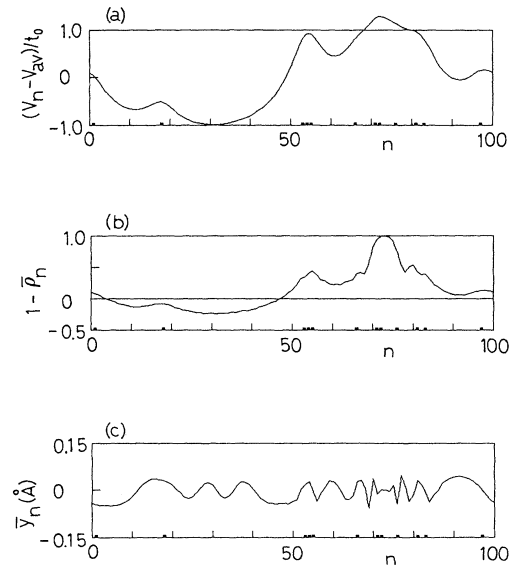

FIG. 3. Quantities $V_n - V_{av}$, $\bar{\rho}_n$, and $\bar{y}_n$ for another sample which is different from those in Figs. 1 and 2. Dielectric constants and the concentration are the same.

more densely. It is smaller where impurity density is lower. The difference between the maximum and minimum of V_n is larger in Fig. 2(a) than in Fig. 1(a). It is the largest in Fig. 3(a). In part (b) of each figure, distribution of the smoothed electron density $\bar{\rho}_n=(\rho_{n-1}+2\rho_n+\rho_{n+1})/4$ is depicted. Instead of $\bar{\rho}_n$, the electron-density reduction from half-filling, $1-\bar{\rho}_n$ (the hole density) is shown. The gross features of spatial variation of $\bar{\rho}_n$ are mainly determined by the distribution of V_n. Small changes and structures come from the presence of solitons and soliton lattices. Part (c) represents the smoothed dimerization amplitude $\bar{y}_n=(-1)^n(y_n-y_{n+1})/2$, the acoustic component being removed. In Fig. 1(c) a positively charged soliton is pinned around impurities at $n=71$ and 76. A positively-charged-soliton lattice is realized in the region $20\lesssim n\lesssim 50$, where impurities are densely distributed. The hole density is continuously large in this region. Where the spatial fluctuation of V_n is larger, the configuration of the lattice is more complicated. In Fig. 2(c) a negatively charged soliton is found at $n\sim 25$. This soliton is confined in the potential valley around the minimum of V_n. In Fig. 3(c) a negatively-charged-soliton lattice is found in the region $10\lesssim n\lesssim 40$, where the impurities are sparsely distributed. This is associated with the enhanced electron density. Furthermore, the local dimerization amplitude almost disappears at $n\sim 72$. Here the hole density is close to unity. This means that π electrons do not exist and the conjugation is locally disrupted. This is due to the fact that the impurity density is so high that V_n is extraordinarily large around $n\sim 72$ (the magnitude of $V_n-V_{\rm av}$ is larger than t_0). In this way the lattice configurations and electron distributions greatly depend on spatial fluctuation of the impurity strength V_n. The possible configuration patterns are very fertile when the fluctuation is large.

When the concentration is small enough, the fluctuation of V_n is suppressed. Most of the lattice and charge configurations are like those of Fig. 1. As the concentration increases, the fluctuation of V_n enhances. This enhancement raises the number of samples which contain various patterns found in Figs. 2 and 3. When $c\sim 0.20$, about half of the samples contain local disruptions of the π conjugation.

The lattice and electron-density configurations for case B are qualitatively similar to those case A. Quantitatively, the fluctuation of V_n is suppressed because of the larger dielectric constants. Then the probability of the occurrence of configuration patterns such as those of Fig. 1 is larger than in case A.

Randomly and independently chosen samples are averaged over $N_{\rm sa}=100$ times for each set of dielectric constants and concentration. Here we tacitly consider a fibril structure which is composed $N_{\rm sa}$ chains of size N. Real fibrils in $(CH)_x$ might have the similar numbers of $N_{\rm sa}$ and N. We numerically simulate electronic and lattice structures of the fibril itself (we do not take the limit, $N_{\rm sa}\rightarrow\infty$). Weak three-dimensional couplings among chains would be present in real systems. We, however, neglect them because it is beyond the capacity of the computer to treat them fully. Results would not change so much as far as the three-dimensional effects are weak enough.

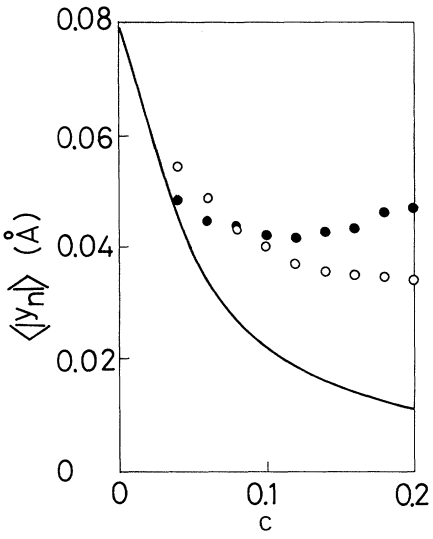

FIG. 4. Concentration dependences of averaged dimerization amplitude $\langle|y_n|\rangle$. The notation $\langle\ \rangle$ indicates averaging over $N_{\rm sa}$ samples and N lattice points in each sample. The solid line shows $\langle|y_n|\rangle$ of the impurity-free soliton lattice system, $I_s=0$. The symbols ● and ○ denote numerical data for cases A and B, respectively.

Figure 4 shows the averaged dimerization amplitude $\langle|y_n|\rangle$, where $\langle\ \rangle$ means the averaging over $N_{\rm sa}$ samples and N sites. Numerical data for cases A and B are denoted by the solid and open circles, respectively. The solid line represents the same quantity $\langle|y_n|\rangle$ of the impurity-free system. The magnitude of $\langle|y_n|\rangle$ of the systems with impurities is larger than that of the impurity-free system. This may come from the fact that the magnitude of the dimerization amplitude in regions far from the solitons, for example, the region $70\lesssim n\lesssim 95$ in Fig. 2, is larger than that of the impurity-free soliton-lattice system. A similar enhancement of $\langle|y_n|\rangle$ has been found in the case of short-ranged site-type impurities.[8] For case A, i.e., the stronger impurity potentials, the absence of decrease for higher concentrations is found. The reason may be that most of the positive solitons are so strongly pinned around large-V_n regions that the soliton width is smaller than that in the impurity-free system, and thus the spatial regions, where the dimerization amplitude takes relatively larger value than in the impurity-free system, extend. The same property has been pointed out in the site-type impurity problem.[8] We conclude that the *dimerization is enhanced by the presence of the long-ranged impurities,* as has been found in the case of the short-ranged impurities. The enhancement means that the magnitude of $\langle|y_n|\rangle$ is larger than that of the impurity-free system, but is not necessarily larger than that of the perfectly dimerized ground state. The dimerization becomes smaller around impurities, but persists more strongly in the regions far from impurities. The latter persistence mainly contributes the enhancement of

$\langle |y_n| \rangle$. This persistence of the bond-alternation pattern agrees with experimental features of heavily doped polyacetylene: For instance, the x-ray-diffraction data have the peak associated with the bond-alternation pattern of double and single bonds [for example, see Fig. 1(b) of Ref. 13].

Next, we discuss the electronic properties. Figure 5(a) shows the density of states of the impurity-free system with $c=0.12$. We show typical simulation data of the density of states per site by a histogram in Fig. 5(b). The dielectric constants are those of case A and the concentration is $c=0.12$. The position of the Fermi level is denoted by the arrow. The randomness has rounded off the inverse-square-root divergences found at band edges in Fig. 5(a). The valence, soliton, and conduction bands are already joined together. The breakdown of the electron-hole symmetry due to the impurity potentials is clearly seen.

In order to obtain information about the electronic structures around the Fermi level, we analyze the data in the following way. For a fixed set of dielectric constants and concentration, the energy gap E_g is defined as the difference between the minimum of eigenvalues of the lowest unoccupied states among the N_{sa} samples and the maximum of those of the highest occupied states. In other words, we assume that the energy gap vanishes in the fibril when the valence- and soliton-band states overlap each other. It is obvious that this definition of E_g explicitly depends on N_{sa}. We, however, believe that this simple definition can be helpful to simulate electronic structures of polyacetylene films which are composed of fibrils with similar magnitudes of N and N_{sa}. As far as $E_g>0$, the Fermi energy of the fibril locates in the energy gap. Weak interchain interactions do not transfer electrons among chains. Then the definition of E_g would be reasonable. On the other hand, when $E_g<0$, the electrons will move among chains due to the interchain couplings. The fibril system will change into energetically more favorable configurations. Eventually, the relation $E_g>0$ will be satisfied. We cannot simulate this situation because of the limited CPU time available. We, however, believe that E_g would become small enough, compatible with the mean level spacing of the undimerized system. Then we could regard the system as metallic. In the present work, we calculate the density of states per site at the Fermi energy $\rho(\mu)$, when $E_g<0$, by the number of states between the minimum and maximum. It is to be divided by the product $NN_{sa}|E_g|$. The result would not change so much even if the three-dimensional transfer is included, because the mean level spacing is so small that the system is regarded as metallic. It should be noted that the same definitions of E_g and $\rho(\mu)$ as those in the previous work[8] are used so as to compare each other's results.

Numerical data about E_g and $\rho(\mu)$ for cases A and B are presented in Figs. 6 and 7, respectively. Solid circles represent the energy gap. When the gap is open, it is E_g. When the gap disappears, the solid circles show the zero value and the solid squares represent $|E_g|$. The density of states at the Fermi level $\rho(\mu)$ is shown by the open cir-

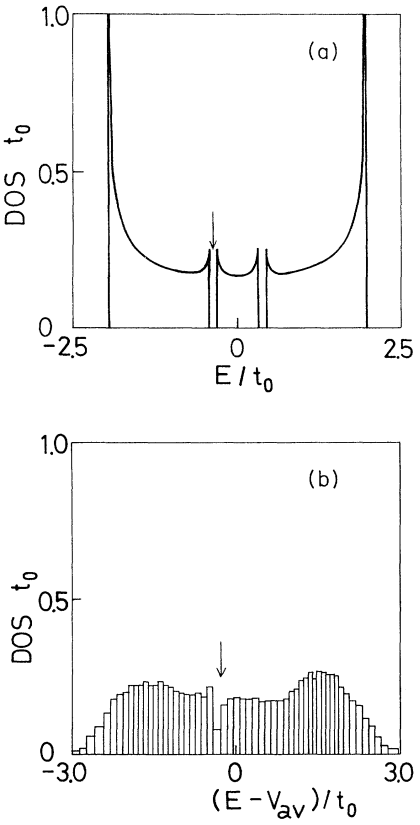

FIG. 5. Densities of states per site (a) for the impurity-free system and (b) for case A. The concentration is $c=0.12$. The arrow shows the position of the Fermi level. In (b) the valence, soliton, and conduction bands are joined together.

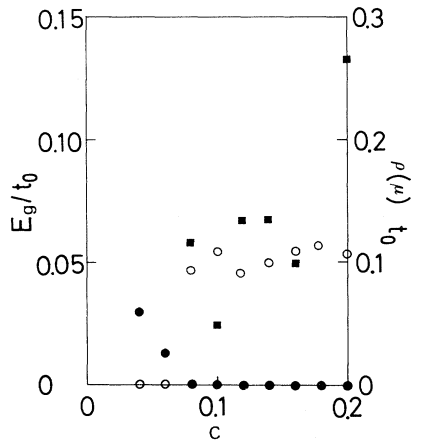

FIG. 6. Impurity concentration dependences of the energy gap and density of states per site at the Fermi level for case A. Numerical data of the energy gap is denoted by solid circles: It is E_g when E_g is positive and zero otherwise. When $E_g<0$ its absolute value $|E_g|$ is shown by the solid squares. The open circles indicate the density of states at the Fermi level $\rho(\mu)$. The left scale represents numerical values of the gap and $|E_g|$, while the right scale is for $\rho(\mu)$. Note that the solid square for $c=0.18$ is out of the range of the left scale; the value is $0.252t_0$.

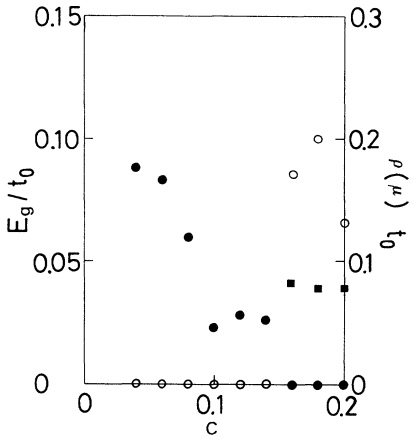

FIG. 7. Impurity concentration dependences of the energy gap and density of states per site at the Fermi level for case *B*. Notations are the same as those in Fig. 6.

cles. We find that the energy gap vanishes between the concentrations $c=0.06$ and 0.08 for case *A*. The critical concentration lies between $c=0.14$ and 0.16 for case *B*. This reflects the difference in magnitudes of dielectric constants, in other words, impurity strengths. The critical concentration of case *A* is close to the observed value, about 7%. The values of $\rho(\mu)$ in the concentration region with no energy gap are of magnitudes similar to that of the impurity-free undimerized system, $(2\pi t_0)^{-1}\simeq 0.16t_0^{-1}$. This explains well the magnitude of the density of states estimated from the observed Pauli susceptibility. To conclude, our results of case *A* remarkably explain observed features of the metal-insulator transition: the value of the critical concentration, the appearance of the Pauli susceptibility, and its magnitude.[12]

We analyze amplitude distributions of wave functions with the help of the inverse participation numbers (IPN's).[14] The IPN of the κth wave function is defined by

$$I_\kappa=\frac{\sum_n|\phi_\kappa(n)|^4}{[\sum_n|\phi_\kappa(n)|^2]^2}\ . \tag{3.1}$$

It is a relative measure of the strength of localization. It is larger when the wave function is more strongly localized. The IPN's for the impurity-free system with $N=100$ and $c=0.12$ are presented in Fig. 8(a). The magnitudes are of plane waves. A characteristic simulation result is shown in Fig. 8(b). The dielectric constants are of case *A* and the concentration is $c=0.12$. $N\times N_{\rm sa}$ points $(\varepsilon_\kappa, I_\kappa)$ are plotted. The arrow indicates the position of the Fermi level. It is at the center in the small interval of the width $|E_g|$. The IPN's of the soliton and conduction bands are like of one band: The states in two band edges are localized more strongly than those in the band center. This indicates that the soliton and conduction bands are so strongly mixed together that they cannot be recognized as two independent bands. On the other hand, the valence and soliton bands do not mix so strongly. This is the consequence of the two facts that the Peierls mechanism, to open a wide gap around the

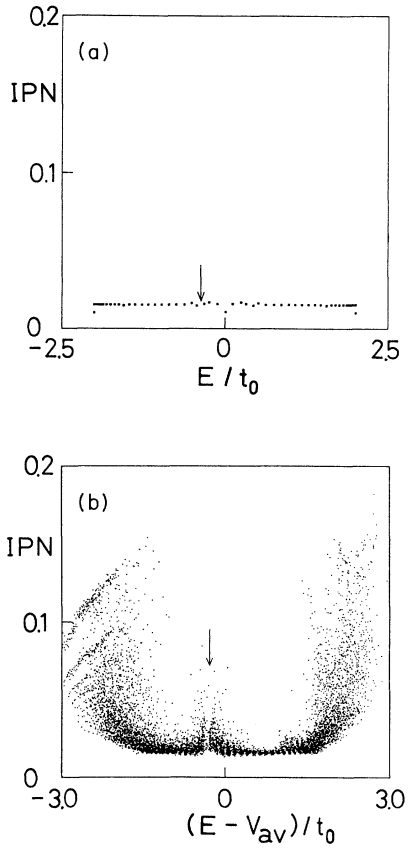

FIG. 8. Inverse participation numbers of wave functions (a) for the impurity-free system and (b) for case *A*. The concentration is $c=0.12$ The arrow indicates the position of the Fermi level. In (b), $N\times N_{\rm sa}$ points $(\varepsilon_\kappa, I_\kappa)$ are plotted.

Fermi level, is effective even in disordered systems and that the electron-hole symmetry property is violated due to the impurity potentials. The IPN's of the valence band are larger than those of the soliton and conduction bands. This asymmetry can be explained by the difference in the number of states and bandwidth between two bands. The number of states in the valence band is smaller than that of the soliton and conduction bands. The width of the valence band is narrower than that of the latter. Thus the IPN's of the states in the middle of the valence band are larger than those in the center of the other bands. The IPN's around the Fermi level are relatively larger than those at the band centers. Wave functions are more strongly localized. This feature may be disadvantageous to explain the metallic conduction. This may reveal limitations of discussions based on one-dimensional models. Higher-dimensional effects might be necessary to discuss the high conductance.

IV. SUMMARY AND DISCUSSION

In the present paper, we have numerically investigated lattice configurations and electronic structures of doped *trans*-polyacetylene, when charged impurities are ex-

pressed by long-ranged Coulomb potentials. The electron number is determined by the number of the impurities. The numerical method is the same as that has been used in our previous work on the short-ranged site-type impurity problem[8] The main conclusions are that the energy gap can vanish at the impurity concentration of several percent even as the bond-alternation patterns persist and are rather enhanced by the impurities. The enhanced dimerization is larger than that in the impurity-free system, but is smaller than that of the perfectly dimerized ground state. These properties do not depend on whether the impurity potentials are short or long ranged. The presence of dimerization in the highly doped case agrees with results of x-ray diffraction experiments, which providing evidence for the alternation of single and double bonds.[13] The disappearance of the energy gap can explain the observed metal-insulator transition characterized by the onset of the metallic Pauli susceptibility. Our calculations are in excellent agreement with the experimental properties: the value of the critical impurity concentration, the appearance of density of states inferred from the Pauli susceptibility, and its magnitude.[12]

We find an interesting correspondence between the short- and long-ranged impurity-potential problems. This is shown in the Appendix. Two quantities, the critical concentration of the energy gap and the correlation between the impurity-potential configuration and electron-density distribution, remarkably agree with each other. This indicates that the electronic properties do not strongly depend on the range of impurity potential. On the other hand, the lattice configuration patterns are affected by whether the impurity-potential range is short or long. For the short-ranged impurity potentials, the local dimerization amplitude around impurities changes suddenly. The lattice configuration patterns contain strongly pinned solitonlike objects. The averaged order parameter is also sensitive to the impurity-potential strength. When the impurity potentials are long ranged, the order parameters around the impurities do not varies so strongly. Thus, the averaged order parameter does not change so much as in the short-ranged impurity-potential problem. The spatial fluctuation in the impurity-potential strength is enhanced compared relative to that in the short-ranged impurity-potential case. The lattice configurations contain various kinds of local objects: positive and negative solitons, positive- and negative-soliton lattices, and disruption of π conjugation. In contrast, only the positive soliton and positive-soliton lattice were found in the short-ranged impurity-potential problem.

From the analysis of IPN's, we find an asymmetry between the valence and conduction bands. The gap between the soliton and conduction bands closes for weak strength of disorder. The gap between the valence and soliton bands is stable against disorders. It vanishes for stronger disorder. Distribution of plots in Fig. 8 reflects this difference. IPN's of the soliton and conduction bands have a structure characteristic of a single band. Their values at the middle part of each band are larger in the valence band. The asymmetry has also been found in the short-ranged impurity-potential problem.[8] It is one of the consequences of the absence of the electron-hole symmetry.

In the present paper, we have mainly discussed the electronic properties of the doped system. Transport properties are yet to be investigated. The reasons are as follows. Solitons are strongly pinned at the peaks and bottoms of the spatial variation of the impurity potential. They cannot participate in the electric conduction in the framework of the one-dimensional model. Higher-dimensional effects, i.e., electron-hopping processes between solitons in different chains, should be taken into account. In addition, interfibril coupling might play an important role because the high conductance is observed over the whole sample. Further evidence, which indicates that the three-dimensional couplings might be necessary, is the fact that the wave functions around the Fermi level are relatively strongly localized as seen in the IPN data. These problems remain to be investigated in the future.

In the present series of works, we have considered the random arrangements of impurities. In highly oriented polyacetylene films, there might be some correlation among distributions of impurities.[13] A metal-insulator transition is observed also in these samples. A possible origin for the correlated distribution is interimpurity interactions.[15] Even if the screening mechanism by electrons in a chain were effective, long-ranged components of the impurity potentials would still remain. An overlap of the long-ranged components due to different impurities would result in interimpurity interactions. This effect has not been included in the present paper. The model (2.1) can be generalized to include interimpurity interactions. Numerical procedures described in Sec. II should be extended to obtain stationary impurity distributions as well as lattice and electron configurations. This problem is to be studied and reported in a separate paper.[16]

ACKNOWLEDGEMENTS

Fruitful discussions with Professor Y. Wada, Professor Y. Ono, and Dr. K. Fesser are acknowledged. This work has partly been financed by a Grant-in-Aid for Scientific Research from the Ministry of Education, Science, and Culture, Japan. Numerical works have been performed on the FACOM M-380Q computers of the International Center for the Elementary Particle Physics, University of Tokyo, on the HITAC M-680 and S-820 computers of the Computer Center of University of Tokyo, and also on the HITAC M-680 and S-820 computers of the Institute of Molecular Science, Okazaki National Research Institutes.

APPENDIX: COMPARISON WITH THE SHORT-RANGED IMPURITY-POTENTIAL PROBLEM

As discussed in Sec. III, we have obtained numerical data which indicate the disappearance of the energy gap with the persisting bond alternation. These properties were found also in the short-ranged site-type impurity-potential problem.[8] It would be interesting to find relations between short- and long-ranged impurity-potential

problems. In this appendix we make a quantitative comparison.

In Ref. 8 we have shown that the energy gap vanishes at the concentration between $c=0.14$ and 0.16 for the site-type strength $I_s=0.8t_0$. This result corresponds to that of case B of this paper. Similarly, the energy gap disappears at the concentration between $c=0.08$ and 0.10 for $I_s=1.2t_0$. The critical concentration for case A in this paper is a little bit smaller than that for $I_s=1.2t_0$. The magnitudes of the local impurity strengths at the center of an impurity of cases A and B are $V(i;i)=0.67t_0$ and $0.44t_0$, respectively. The ratio between the two values is $0.67t_0/0.44t_0=1.52$. This is very close to the ratio of the two site-type impurity strengths, $1.2t_0/0.8t_0=1.50$. In the previous study,[8] we have discussed that the effective short-ranged site-type strength may be a quantity integrated over several sites around a center of an impurity. Therefore, the effective value of the short-ranged strength can be several times of the local value of the long-ranged potential. The above comparison confirms this speculation: The local strength $0.44t_0$ for case B corresponds to the site-type strength $I_s=0.8t_0$. The effective site-type strength of the local strength $0.67t_0$ for case A can be a little bit larger than $I_s=1.2t_0$.

The correspondence discussed in the previous paragraph is based on a comparison of the electronic structures. For the order parameter, which measures the dimerization amplitude, the corresponding impurity strength can be different. In fact, the averaged order parameters of A and B in Fig. 4 are like those of the site-type strength in the region $0.4<I_s/t_0<0.8$ in Ref. 8. This can be explained in the following way. For the site-type impurities, the impurity acts on electrons only at the one lattice site, and thus the width of the pinned soliton becomes much shorter than that of the free solitons. Then the order parameter far from the impurity and the soliton can become much larger. This results in the large change of the averaged order parameter. On the other hand, for the long-ranged impurity potentials, the soliton width does not change so much as in the short-ranged impurity-potential problem. Thus the averaged order parameter changes only weakly. In this way the average order parameters do not necessarily take similar values, even if the electronic structures of the long- and short-ranged impurity-potential problems resemble each other. This is the consequence of the fact that effective ranges of impurities are different for both problems. However, the remarkable feature that the bond-alternation pattern is enhanced by the impurities is common to both problems.

Furthermore, we compare the two problems with the help of a correlation function. We consider impurity-potential effects on the spatial distribution of electron density. For the long-ranged impurity-potential problem, we shall calculate a correlation $\langle F\rangle$, between the potential strength at the nth site V_n and the electron distribution ρ_n as follows:

$$\langle F\rangle=\langle(V_n-V_{\rm av})(\rho_n-\rho_{\rm av})\rangle\ , \tag{A1}$$

where $\rho_{\rm av}=(1/N)\sum_n\rho_n$. Equation (A1) is transformed

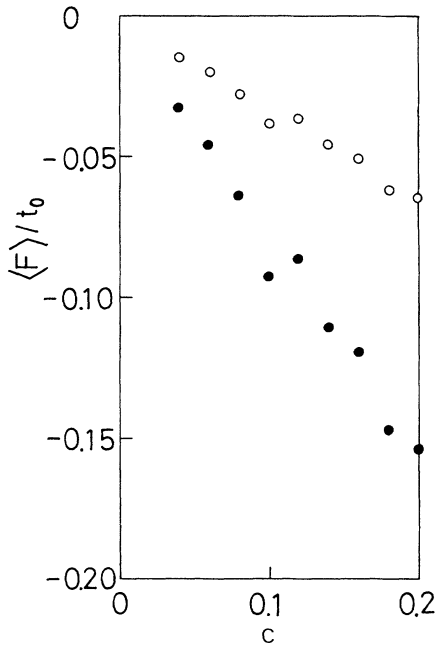

FIG. 9. Concentration dependences of the correlation $\langle F\rangle$ for the present long-ranged impurity-potential problem. The solid and open circles denote numerical data for cases A and B, respectively.

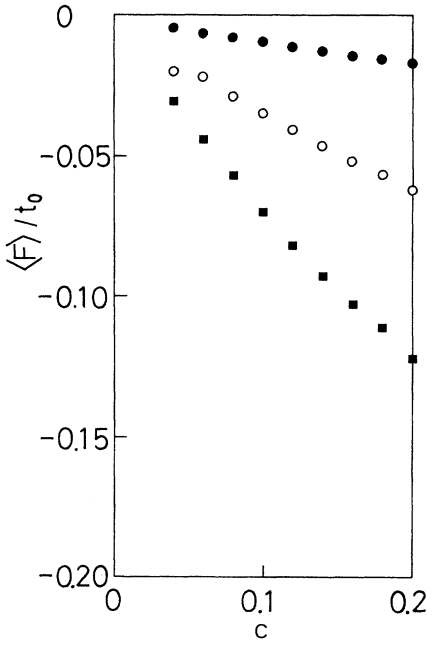

FIG. 10. Concentration dependences of the correlation $\langle F\rangle$ for the previous short-ranged impurity-potential problem. The solid circles, open circles, and solid squares represent numerical data for $I_s/t_0=0.4$, 0.8, and 1.2, respectively. Here, I_s is the strength of the short-ranged site-type impurity potential.

into

$$\langle F \rangle = \langle V_n(\rho_n - \rho_{\rm av}) \rangle \ . \tag{A2}$$

Then the quantity $\langle F \rangle$ also has the meaning of energy difference per site of the impurity-potential terms between the energetically optimized electron distribution and the ideal uniform distribution. Numerical results of $\langle F \rangle$ are shown as functions of the concentration in Fig. 9. Results for cases A and B are denoted by solid and open circles, respectively. The quantity $\langle F \rangle$ is negative. This indicates that local electron density is small when the potential strength is large. It is large when the potential strength is small. The decrease of $\langle F \rangle$ is almost a linear function of the concentration c. The decrease is stronger for case A, because of the larger impurity strength. In the same way, we define the quantity $\langle F \rangle$ for the site-type impurity-potential problem as follows:

$$\langle F \rangle = \left\langle \left[I_s \sum_i \delta_{i,n} - cI_s \right] (\rho_n - \rho_{\rm av}) \right\rangle \ . \tag{A3}$$

Here the sum with respect to i is taken over all the impurity positions. Figure 10 shows the results calculated from the numerical data given in Ref. 8. The quantities $\langle F \rangle$ for $I_s/t_0 = 0.4$, 0.8, and 1.2 are denoted by solid circles, open circles, and solid squares, respectively. Their decrease as functions of c is nearly linear. Comparing Figs. 9 and 10, we find that data for case B and $I_s = 0.8t_0$ remarkably agree. This suggests that impurity effects on electron distribution in both systems are of the same extent. As discussed previously, the critical concentration where the gap vanishes is common to the two systems. It would be very interesting to point out that we can make correspondence between the long- and short-ranged impurity-potential problems by two quantities, i.e., the correlation function $\langle F \rangle$ and critical concentration, although the relation between the two quantities is not clear in the present simulation work. The decrease of $\langle F \rangle$ for case A in Fig. 9 is a little bit stronger than that for $I_s = 1.2t_0$ in Fig. 10. Thus the impurity effects on the electron distribution are slightly stronger for case A than for $I_s = 1.2t_0$. It is also interesting to point out that the critical concentration of the electronic gap for case A is a little bit smaller than that for $I_s = 1.2t_0$. In this way the strength of disorder effects on the electron-density distribution is closely related to the strength of impurity effects on the electronic structure.

*Present address: Fundamental Physics Section, Physical Science Division, Electrotechnical Laboratory, Umezono 1-1-4, Tsukuba, Ibaraki 305, Japan.

[1]K. Harigaya, Y. Wada, and K. Fesser, Phys. Rev. Lett. **63**, 2401 (1989).

[2]K. Harigaya, Y. Wada, and K. Fesser, Phys. Rev. B **42**, 1268 (1990).

[3]K. Harigaya, Y. Wada, and K. Fesser, Phys. Rev. B. **42**, 1276 (1990).

[4]K. Harigaya, J. Phys. Soc. Jpn. **59**, 1348 (1990).

[5]K. Harigaya, Y. Wada, and K. Fesser, Phys. Rev. B **42**, 11 303 (1990).

[6]K. Harigaya, Y. Wada, and K. Fesser, in *Strongly Coupled Plasma Physics,* edited by S. Ichimaru (Elsevier Science/Yamada Science Foundation, New York, 1990), p. 255; Synth. Met. **43**, 3579 (1991).

[7]K. Harigaya, A. Terai, Y. Wada, and K. Fesser, Phys. Rev. B **43**, 4141 (1991).

[8]K. Harigaya and A. Terai, Synth. Met. **43**, 3481 (1991); Solid State Commun. **78**, 335 (1991).

[9]H. Takayama, Y. R. Lin-Liu, and K. Maki, Phys. Rev. B **21**, 2388 (1980).

[10]W. -P. Su, J. R. Schrieffer, and A. J. Heeger, Phys. Rev. B **22**, 2099 (1980).

[11]E. M. Conwell and S. Jeyadev, Phys. Rev. Lett. **61**, 361 (1988); E. M. Conwell, H. A. Mizes, and S. Jeyadeve, Phys. Rev. B **40**, 1630 (1989); **41**, 5067 (1990).

[12]A. J. Heeger, S. Kivelson, J. R. Schrieffer, and W. -P. Su, Rev. Modd. Phys. **60**, 781 (1988).

[13]N. S. Murthy, L. W. Shacklette, and R. H. Baughman, Phys. Rev. B **41**, 3708 (1990).

[14]P. Dean and R. J. Bell, Discuss. Faraday Soc. **59**, 55 (1970).

[15]R. J. Cohen and A. J. Glick, Phys. Rev. B **40**, 8010 (1989).

[16]K. Harigaya, J. Phys. Condens. Matter (to be published).